BJES Basrah Journal for Engineering Sciences

Basrah Journal for Engineering Sciences, Vol. 21, No. 2, (2021), 17-28

Original Article

Journal homepage: www.bjes.edu.iq
ISSN (Online): 23118385, ISSN (Print): 18146120

OPEN ACCESS

Experimental, Theoretical and CFD Validations for Solar Powered Atmospheric Water Generation Using Thermoelectric Technics

Mohammed Alsheekh [1,*], Saleh E. Najim [2], Hussein S. Sultan [3]

[1,2,3] *Department of Mechanical Engineering, College of Engineering, University of Basrah, Basrah, Iraq*
E-mail addresses: mohammed.sadkhan@uobasrah.edu.iq , pro.salehnajim52@gmail.com , hussein.sultan@uobasrah.edu.iq
Received: 25 August 2020; Accepted: 14 February 2021; Published: 11 July 2021

Abstract

The Atmospheric Water Generator (AWG) is an environmental water recovery that easily dehumidifies water vapor moisture from the air. This article presents an experiment to construct an AWG model using solar energy as a source of power. An experimental and numerical study for a device of (AWG) is performed. The experimental work is performed at Basrah city, located in the south of Iraq, during August and September of 2019 and March of 2020. The theoretical results are calculated by EES and the numerical study has been conducted by the (ANSYS19/CFD/ FLUENT) program. The experimental device is tested for different days with different climate conditions. The Maximum water production obtained is 3.4 L/day from all the testing days, for different hours of operation when the relative humidity in the range of (45 – 95 %) and the temperature range from 17 °C to 45 °C. The results shown that, the water production rate is increased with increasing humidity, temperatures, hours of operation, and model size.

Keywords: AWG, TEC, Thermoelectric, Soler Energy, CFD/ANSYS/ FLUENT.

http://dx.doi.org/10.33971/bjes.21.2.4

1. Introduction

Potable water shortages are one of the most pressing issues in the world today. Although water covers more than two-thirds (71 %) of the earth's surface, the amount of water suitable for daily use is still scarce (approximately 2.75 %). Long coastal countries and island countries often face water scarcity with inadequate freshwater supplies, such as rivers and pools. Alternative ways of producing water to meet water requirements needs are urgently needed. The relative humidity is very high in coastal areas, which can be used to dehumidify water [1]. Scrivani and Ugo (2008) [2], investigated a project's aims to explore solar concentrating plants in Mediterranean countries to supply renewable water. Their method used is water extraction from the air by direct cooling of humid air below the dew point. Bogardi et al. (2012) [3], studied the sustainability, fair distribution, and conservation of water resources must occur within integrated water management and governance, but their implementation is problematic. Continuing global climate change, growing population, urbanization, and striving for better living conditions pose a challenge to planetary sustainability. Dash and Anshuman (2015) [4], studied the ability on using dehumidification techniques for supplying potable water for the people in the coastal regions. Since the relative humidity is high in coastal areas (around 70-80 percent) and the sun shines in these places all year. They recommended that dehumidification devices can be used with solar energy as a power source. Kabeel et al. (2016) [5], investigated the technique was intended for Arab Gulf nations and comparable countries by utilizing sun-oriented thermometric generator usage. Cases have been simulated in 3D using CFD programming. It found that the freshwater efficiency of the unit was up to 3.9 L/h/m^2. Liu et al. (2017) [6], designed and experimentally investigated a portable water generator of (7 kg) capacity with two thermoelectric coolers (TECs). They found that, the amount of generated water increased with airflow rates rose, but the condensation rate had the opposite trend. Bharath et al. (2017) [7], studied an atmospheric Water Generator (AWG); this device can convert atmospheric moisture into potable water. The device uses the principle of latent heat to convert water vapor molecules into water droplets with Peltier devices' help. The CFD analysis is carried out to optimize the design by changing Peltier's number and Peltier's location to the desired condensing temperature. Islam et al. (2017) [8], investigated Bangladesh's coastal areas and found the humidity was very high (around 70-80 percent). If enough dehumidifier units are used in an environment individually could meet their water needs. The present study implemented a technique to set up an A.C. concept based on a thermo-electric cooler that used 12 volts D.C. In this cooler, the water has been removed from the air by directly cooling moist air below the dew point. And the possibility of using the sun-powered cooling framework to provide the required cooling force was investigated. The water produced by design must be compatible with the World Health Organization (WHO); the design should not danger to users during regular operation. The flexibility in the energy source and the design should be able to use various energy sources.

The aim of this study to develop, test, and simulate atmospheric water generation device. The unit condenses the water vapor present in the atmosphere and then purifies it to accommodate human use. When designing the atmospheric water generator, the required specifications are defined to ensure that it fulfills its intended function.

2. Experimental work

2.1. Components of the device

The components used for the construction of the water generation device are as shown below:

Table 1. the parts of the model of paper.

Item No.	Component name	QTY	Specification	City	Fig No.
1	A draft fan in the cooled side	2	DC 12 V 0.16 Amp.	China	2
2	Draft fan in hot side	1	12 V DC	China	4
3	Peltier	3	TECI-12715	China	4
4	Cover	1	Plastic sheet	Locally	1
5	Casing	1	Insulated plastic	Locally	1
6	Battery	1	60 Ah 12 V DC	Korea	1
7	Solar cell	1	MODEL: SY-S060 W	China	1

2.2. Description of the device

The housing is split into 3 chambers. The inlet air is moved to the lower section via the left area, where it comes into contact with the Peltier system's cold surface. Thus, the ambient air inlet loses heat, and its temperature decreases to the TDP and thus begins to condense water vapor. Then the dehumidified air is expelled from the proper chamber from the device. The lower portion also functions as a collecting unit for water. Condensed water vapor is collected in a lower amount by dripping action from the bottom part, while the gravitational force forces down water droplets. It can be seen as given in Figs 1, 2, 3, 4, 5 and 6.

Fig. 1 Details of system No.1

Fig. 2 the sketch of a draft fan in the cooled side.

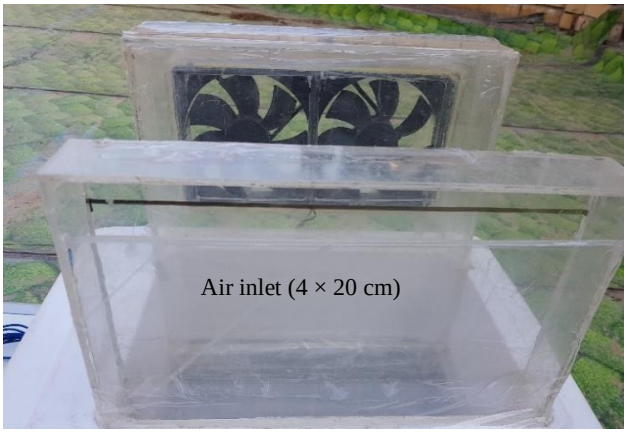

Fig. 3 Details of an inlet of the air.

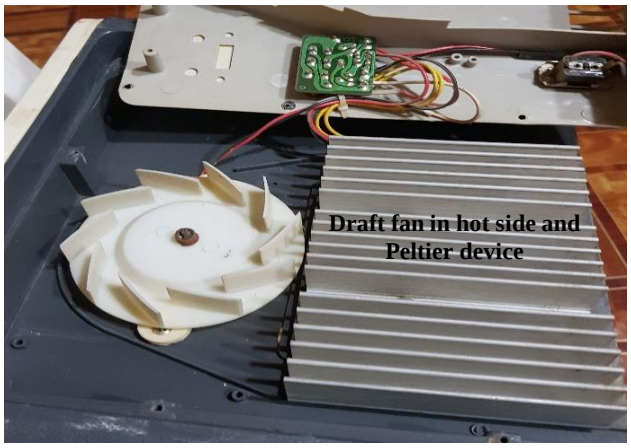

Fig. 4 Details of a Draft fan on the hot side.

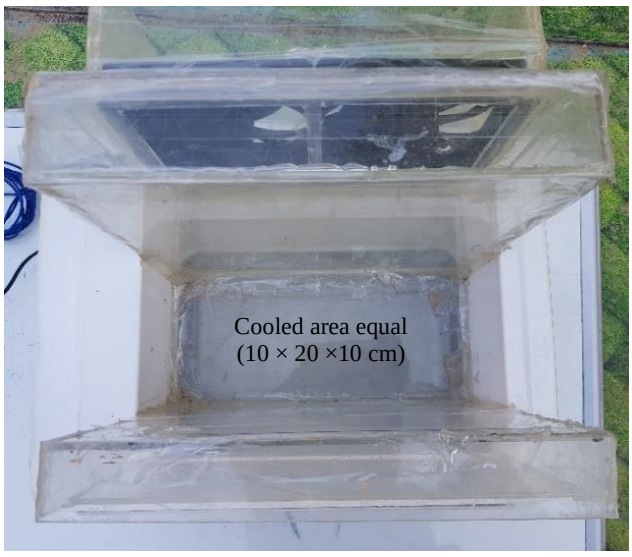

Fig. 5 details of cooled area.

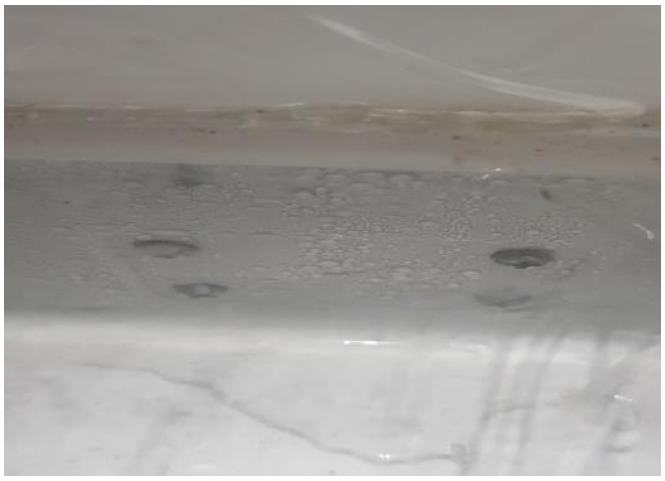

Fig. 6 Actual Picture during Activities.

2.3. Measuring instruments

The experiments used during the experiments are anemometer-psychometry, infrared thermometer, and temperature-humidity meter, as shown in Fig. 7.

Fig. 7 Measuring instruments.

3. Theoretical analysis

The underlying technology that allows the creation of these thermoelectric assemblies is now referred to as the Peltier Effect, it uses two parts of a semiconductor. Upon application of a direct current (D.C.) power supply, these systems produce a cooling operation, counteracted by heat production on the opposite side of the device. Peltier assemblies utilize thermoelectric modules sandwiched between high-performance aluminum heat sinks and one or more high axial fans. Peltier's bodies combined with a proprietary mechanical architecture are designed to pump heat from the enclosure's interior to the outside without exposing sensitive electronics to any outside air or pollution [7]. Proper packaging is shown in Figs. 8 (a) and (b).

For theoretical prediction of available water vapor in the air, the following relations give the necessary dew point temperature required for water vapor condensation, which is accomplished by the Peltier gadget for different temperature and relative humidity:

$$\beta\,(T, RH) = ln\left(\frac{RH}{100}\right) + \frac{aT}{b+T} \tag{1}$$

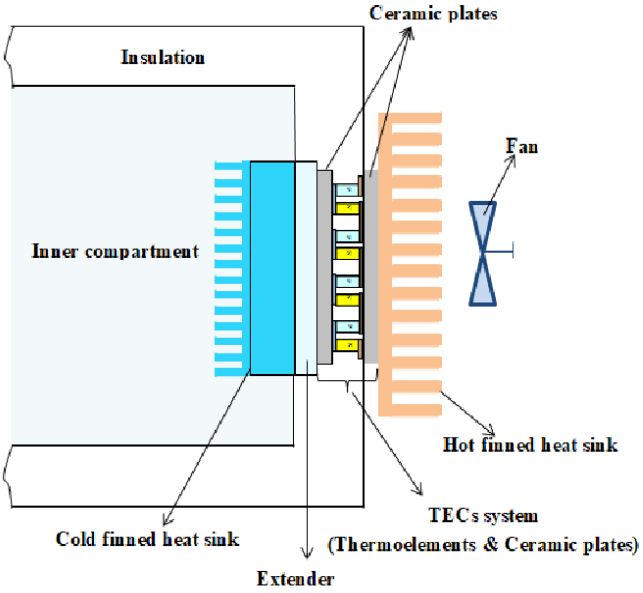

(a)

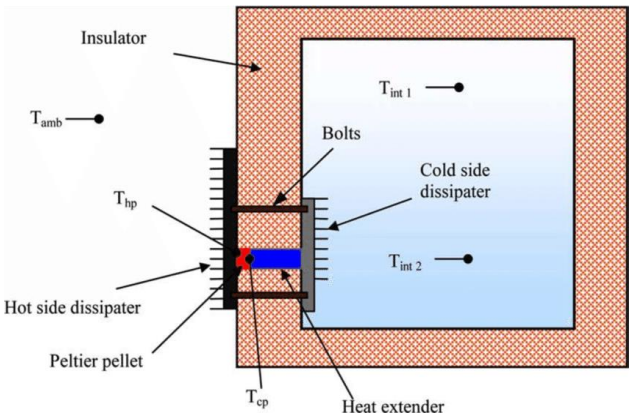

(b)

Fig. 8 sample of diagrams for Peltier's devices.

$$T_{dp} = \frac{b\,\beta\,(T, RH)}{a\ -\ \beta\,(T, RH)} \tag{2}$$

Where: a = 17.67, b = 243.5 and T is in °C.

The ratio of (mv/ma) is defined as humidity ratio denoted by the term of (W), is the mass of vapour associated with one kilogram of dry air, also known as mixing ratio or moisture content and is given by [8]:

$$W = \frac{V_{as}}{V_s} = \frac{287\,(273 + t_d)}{(P_b\ -\ P_s)V_s} \tag{3}$$

Where t_d is the saturation temperature, and Ps is the partial pressure of air, then the moisture content is given by:

$$W_s = 0.622\ \frac{P_s}{(P_b - P_s)} = \frac{kg}{kg}\text{of dry air} \tag{4}$$

Where,

Ws : moisture required to saturate 1 kg of dry air.

Ps : saturated pressure of vapor corresponding to dry bulb temperature from the steam table.

3.1. Boundary Conditions

According to the experimental cases, model configurations concerning boundary and initial conditions and settings of the cases studied are given below.

Table 2. the boundary conditions.

No.	Boundary Conditions	Details
1	Inlet B.C. (Momentum)	air inlet of Figs. 15, 16, three different values of mean axial supply X-velocity are studied, which are (0.25, 0.5, 0.75 m/s) and turbulence intensity of 5 %.
2	Inlet B.C. (Thermal)	Eight values for inlet air temperature are studied, which are (287 K, 293 K, 298 K, 303 K, 308 K, 313 K, and 318 K).
3	Outlet B.C. (Momentum)	Gauge pressure (pascal).
4	Outlet B.C. (Thermal)	Eight different values of outlet temperature are studied, which are (283 K, 289 K, 294 K, 299 K, 304 K, 309 K, and 314 K).
5	Wall B.C.	Stationary wall and no-slip and adiabatic.
6	Peltier B.C. (Momentum)	Stationary wall and no-slip.
7	Peltier B.C. (Thermal)	Temperature (278 K - 283 K).

3.2. Simulation using ANSYS-19 (CFD) code

The theoretical simulation of the experimental device is performed using the ANSYS-19 software. Solving the time-averaged conservation equations of mass, momentum, energy, and chemical species in steady three-dimensional flows:

$$\frac{\partial}{\partial t}(\rho \emptyset) + div\left\{(\rho v \emptyset) - \left(\Gamma_{\emptyset}\ grad_{\emptyset}\right)\right\} = S_{\emptyset} \quad (5)$$

Where, ρ, v, $\Gamma_{\emptyset}$, and $S_{\emptyset}$ are density, velocity vector, effective exchange coefficient of $\emptyset$, and source rate per unit volume, respectively. The domain's discretization is accompanied by reducing the previous equations to their finite domain form using the coefficients' hybrid approximation. The solution method utilizes the simplest algorithm (an improved version of the well-known simple algorithm). The standard (k-ε) turbulence model is applied, while buoyancy effects are considered to improve convergence under relaxation which was used [3], [9].

3.3. TDS Testing

Comparison of the TDS of the produced water by the experimental system with the liquefaction water and the mineral water (R.O.). The TDS method is shown in Fig. 9. In such a case after filtration, the purity of the water created by air is sufficient, and it can be used and processed by adding safe mineral salts to be drinkable.

Generation water from air filtration and pure. TDS = 48	Generation water from the air. TDS = 58	Mineral water R.O. TDS = 83	Liquefaction water. TDS = 591

Fig. 9 actual picture during activities attested.

3.4. Grid Validation

The model has imported to ANSYS-19 workbench from design modular as per the dimensions of draft fan in the cooled side (10 × 20 cm), air inlet (4 × 20 cm), cooled area equal (10 × 20 × 10 cm), which can be seen in Fig. 15. Then meshing is done as per nodes = 209053, elements = 186178, and mesh metric as skewness, min = 1.3057293693791 E-10, max = 0.634146311139607, average = 1.51636138014358 E-03, standard deviation = 2.09977656708668 E-02, as shown in Fig. 16.

3.5. Solution Procedure

The solution procedure included fluent launcher, general, models, materials selection, air properties, boundary conditions, reference values, solution methods, solution initialization, run calculation, and solution convergence as shown in Fig. 17. Included ANSYS CFD post as results for inlet temperatures, outlet temperatures, different velocities, and humidity.

4. Results and Discussion

In this section, the obtained results will be viewed. Firstly, the experimental results have been taken in August and September during 2019 and Spring 2020. The number of experiments performed is 90. The time required for each experiment is three-hour at minimum to 21 hours at maximum during the day of operation, the variation of dry temperature from 17 ℃ to 45 ℃, and the variation of relative humidity from 25 % to 98 %, but in this work chosen from 60 % to 90%. The theoretical prediction for the variation of water vapor content in the air for different dry bubble temperatures and relative humidity is also given to verify and compare it with experimental results. Finally, the results of ANSYS/Fluent simulation for other cases of water generation device are shown as follows:

4.1. Case 1 (Experimental Case)

Actual operation tests for water generation device had been performed for two months in 2019 and one month in 2020 (from 1 August 2019 to 30 September 2019) and (1 March 2020 to 31 March 2020). The range of relative humidity between (60 % - 90 %) and temperature between (17 ℃-45 ℃) has been chosen so that water is collected every hour, representing the amount of water within one day for the

indicated temperatures humidity. The range of water production rate for the experiments performed in August and September from 2019 is from 0.4 L/day to 3.4 L/day, as shown in Table 7, which is suitable for the experimental size device. The water production rate is increased with an increase in humidity at the range of temperatures available. The content of water production rate for the experiments that were performed in spring from 2020 is from 232.2 mL/day to 1323.6 mL/day, as shown in Table 6 and Fig. 13, which is suitable for the size of the experimental device. All the experiments are done using just three of Peltier's elements. The humidity in the air is not the same every time, and the conditions are not even similar, so the amount of water produced is not the same. The variation of water production rate with relative humidity and temperature is shown in the Tables 3, 4 and 5 and Figs. 10, 11, and 12.

The water production rate for constant dry bulb temperature increased with increasing the relative humidity from the tables. Also, the water production rate for constant relative humidity increased with increasing the dry bulb temperature. For high values of relative humidity and dry bulb temperature, increasing the hours of operation led to expanding the water production rate.

Table 3. the amount of water present at different temperature and different *R.H.* according to production 5 hours.

day	Time (h)	Exp. *DBT* (°C)	Exp. *DPT* (°C)	Exp. *R.H.* (%)	Production *mL/h*
7 March 2020	03:00 am	19	11	61	47.0
	04:00 am	19	11	61	47.0
	05:00 am	18	11	63	46.1
	06:00 am	18	11	63	46.1
	07:00 am	19	11	60	46.0
Amount of production for the day according to production 5 hours					232.2

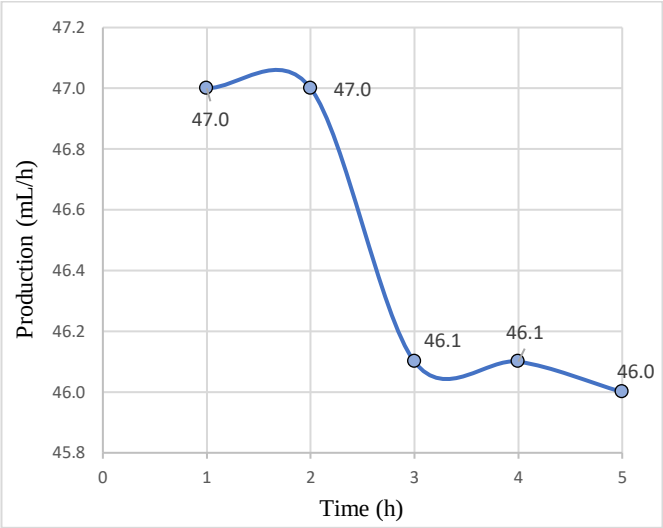

Fig. 10 the amount of water present at different temperature and different *R.H.* according to production 5 hours.

Table 4. the amount of water present at different temperature and different *R.H.* according to production 17 hours.

day	Time (h)	Exp. *DBT* (°C)	Exp. *DPT* (°C)	Exp. *R.H.* (%)	Production *mL/h*
15 March 2020	12:00 am	19	16	84	64.7
	01:00 am	19	16	84	64.7
	02:00 am	18	16	86	63.2
	03:00 am	18	16	89	65.5
	04:00 am	18	16	88	64.7
	05:00 am	18	16	89	65.5
	06:00 am	18	16	85	62.5
	07:00 am	18	15	83	61.0
	08:00 am	19	16	80	61.6
	09:00 am	21	15	70	61.2
	10:00 am	22	15	61	55.4
	06:00 pm	22	15	62	56.3
	07:00 pm	21	15	69	60.3
	08:00 pm	21	15	71	62.1
	09:00 pm	20	16	77	62.0
	10:00 pm	20	16	78	62.8
	11:00 pm	19	15	80	61.6
Amount of production for the day according to production 17 hours					1055.2

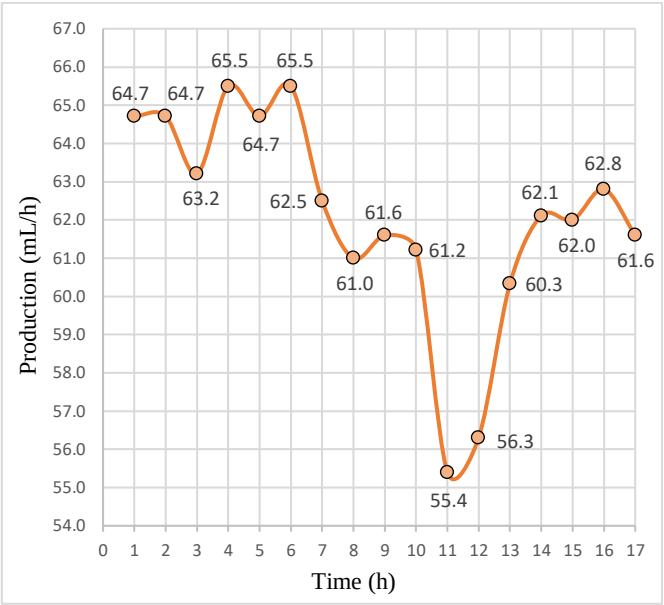

Fig. 11 the amount of water present at different temperature and different *R.H.* according to production 17 hours.

Table 5. the amount of water present at different temperature and different *R.H.* according to production 21 hours.

day	Time (h)	Exp. *DBT* (°C)	Exp. *DPT* (°C)	Exp. *R.H.* (%)	Production *mL/h*
18 March 2020	12:00 am	21	14	66	57.7
	01:00 am	20	14	68	54.6
	02:00 am	20	14	69	55.4
	03:00 am	20	15	72	57.9
	04:00 am	21	16	73	63.9
	05:00 am	20	16	77	62.0
	06:00 am	20	16	80	64.4
	07:00 am	19	16	82	63.1
	08:00 am	20	17	81	65.2
	09:00 am	22	16	72	65.6
	10:00 am	23	16	67	65.7
	11:00 am	23	16	66	64.7
	12:00 pm	23	16	62	60.7
	01:00 pm	24	16	63	66.2
	05:00 pm	24	16	61	64.1
	06:00 pm	23	16	65	63.7
	07:00 pm	22	16	69	62.8
	08:00 pm	22	16	73	66.5
	09:00 pm	21	17	77	67.5
	10:00 pm	21	17	78	68.4
	11:00 pm	20	16	79	63.6
Amount of production for the day according to production 21 hours					1323.8

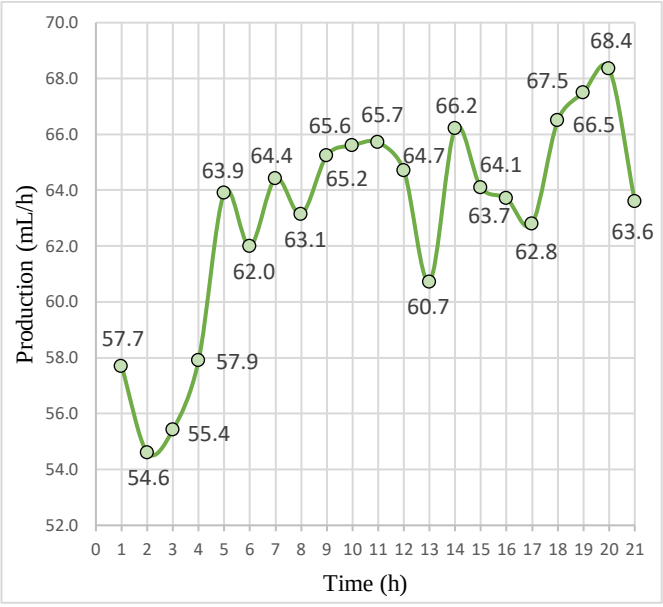

Fig. 12 the amount of water present at different temperature and different *R.H.* according to production 21 hours.

Table 6. the amount of water present at different temperatures and different *R.H.* according to production hours.

No.	Day	Production hours	Average Exp. *DBT* (°C)	Average Exp. *DPT* (°C)	Average Exp. *RH* (%)	Amount of Production for day according to production hours
1	7/3/2020	5	19	11	62	232.2
2	9/3/2020	7	16	9	65	279.4
3	15/3/2020	17	19	16	78.6	1055.2
4	16/3/2020	14	19	15	79	814.2
5	17/3/2020	10	18.6	14	77.1	571.7
6	18/3/2020	21	21.4	16	71	1323.6
7	19/3/2020	11	18.2	13	74	592.9
8	20/3/2020	11	17.6	11	67	511.7
9	22/3/2020	10	16.2	10	67	426.1
10	25/3/2020	9	16.4	12	76	440.0
11	26/3/2020	11	18.6	13	71	684.8
12	27/3/2020	11	19.4	15	75	646.5
13	28/3/2020	14	21	15	68	824.1
14	29/3/2020	12	20	15	75	732.4
15	30/3/2020	11	18.4	14	75	606.2
16	31/3/2020	9	18	13	71	457.3

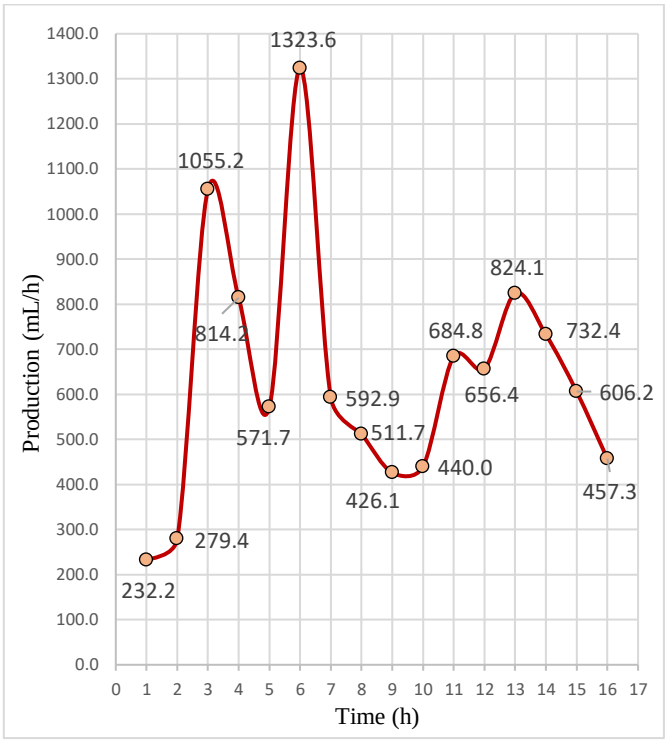

Fig. 13 the amount of water present at different temperatures and different *R.H.* according to production hours.

Table 7. the amount of water present at different Average Humidity Rates according to production hours.

Exp. Day	Exp. Hours	Average Humidity Rate (%)	Amount of water produced (L)
10 / 8 / 19	12	67	1.5
11 / 8 / 19	7	68	0.9
12 / 8 / 19	5	69	0.6
13 / 8 / 19	7	72	0.9
14 / 8 / 19	3	73	0.4
15 / 8 / 19	17	82	2.6
16 / 8 / 19	14	85	2.2
17 / 8 / 19	10	85	1.6
18 / 8 / 19	21	87	3.4
19 / 8 / 19	11	86	1.8
20 / 8 / 19	11	90	1.8
21 / 8 / 19	10	92	1.7
22 / 8 / 19	11	88	1.8
23 / 8 / 19	10	81	1.5
24 / 8 / 19	9	71	1.2
25 / 8 / 19	11	61	1.2
26 / 8 / 19	11	63	1.3
27 / 8 / 19	14	66	1.7
28 / 8 / 19	12	69	1.5
29 / 8 / 19	11	83	1.7
30 / 8 / 19	9	80	1.3
01 / 9 / 19	10	70	1.3
02 / 9 / 19	6	61	0.7
03 / 9 / 19	5	62	0.6
04 / 9 / 19	7	69	0.9
05 / 9 / 19	3	71	0.4
06 / 9 / 19	17	71	2.2
07 / 9 / 19	14	75	1.9
08 / 9 / 19	10	74	1.4
09 / 9 / 19	21	78	3.0
10 / 9 / 19	11	77	1.6
11 / 9 / 19	11	85	1.7
12 / 9 / 19	10	87	1.6
13 / 9 / 19	11	86	1.8
14 / 9 / 19	10	75	1.4
15 / 9 / 19	9	63	1.0
16 / 9 / 19	8	63	0.9
17 / 9 / 19	7	65	0.8
18 / 9 / 19	6	65	0.7
19 / 9 / 19	5	68	0.6
20 / 9 / 19	4	67	0.5
21 / 9 / 19	6	72	0.8

4.2. Case 2 (Theoretical Case)

Theoretical predictions for the dew point temperature obtaining by the Peltier gadget and the percentage of moisture and the amount of water in the metric square of air will be viewed. The calculations are performed for different values of relative humidity and dry bulb temperature in the range of (45-100 %) and (15-50 °C), respectively. The results are given in Tables 8, 9, 10, 11, and 12 and Fig. 14. The theoretical predictions are consistent with the experimental results. The behavior is the same as that of the experimental results for increasing the water production with increasing the temperature and relative humidity.

Table 8. the amount of water present in 1 m^3 in different temperatures with 55 % *R.H*.

Temp. (°C)	Saturation Pressure (bar)	Relative Humidity (*RH* %)	Partial Pressure of water (bar)	Humidity Ratio	Amount of water (L/m^3 air)
25	0.032	55	0.0176	0.010995028	10.995028
26	0.034	55	0.0187	0.011695139	11.695139
27	0.036	55	0.0198	0.012396799	12.396799
28	0.038	55	0.0209	0.013100015	13.100015
29	0.04	55	0.022	0.013804792	13.804792
30	0.042	55	0.0231	0.014511135	14.511135
31	0.045	55	0.02475	0.015573596	15.573596
32	0.048	55	0.0264	0.016639611	16.639611
33	0.05	55	0.0275	0.01735227	17.35227
34	0.053	55	0.02915	0.018424246	18.424246
35	0.056	55	0.0308	0.019499822	19.499822
36	0.059	55	0.03245	0.020579017	20.579017
37	0.063	55	0.03465	0.022023605	22.023605
38	0.066	55	0.0363	0.023111316	23.111316
39	0.07	55	0.0385	0.024567325	24.567325
40	0.074	55	0.0407	0.026029921	26.029921
41	0.078	55	0.0429	0.02749915	27.49915
42	0.082	55	0.0451	0.028975056	28.975056
43	0.087	55	0.04785	0.030829397	30.829397
44	0.091	55	0.05005	0.032320494	32.320494
45	0.096	55	0.0528	0.034193972	34.193972

Table 9. the amount of water present in 1 m^3 in different temperatures with 65 % *R.H*.

Temp. (°C)	Saturation Pressure (bar)	Relative Humidity (*RH* %)	Partial Pressure of water (bar)	Humidity Ratio	Amount of water (L/m^3 air)
25	0.032	65	0.0208	0.013036022	13.036022
26	0.034	65	0.0221	0.01386894	13.86894
27	0.036	65	0.0234	0.014704046	14.704046
28	0.038	65	0.0247	0.015541348	15.541348
29	0.04	65	0.026	0.016380856	16.380856
30	0.042	65	0.0273	0.017222577	17.222577
31	0.045	65	0.02925	0.018489329	18.489329
32	0.048	65	0.0312	0.019761112	19.761112
33	0.05	65	0.0325	0.020611777	20.611777
34	0.053	65	0.03445	0.021892011	21.892011
35	0.056	65	0.0364	0.023177356	23.177356
36	0.059	65	0.03835	0.024467843	24.467843
37	0.063	65	0.04095	0.026196544	26.196544
38	0.066	65	0.0429	0.02749915	27.49915
39	0.07	65	0.0455	0.029244123	29.244123
40	0.074	65	0.0481	0.030998498	30.998498
41	0.078	65	0.0507	0.03276235	32.76235
42	0.082	65	0.0533	0.034535757	34.535757
43	0.087	65	0.05655	0.036766071	36.766071
44	0.091	65	0.05915	0.038561262	38.561262
45	0.096	65	0.0624	0.040819057	40.819057

Table 10. the amount of water present in 1 m^3 in different temperatures with 80 % *R.H*.

Temp. (°C)	Saturation Pressure (bar)	Relative Humidity (*RH* %)	Partial Pressure of water (bar)	Humidity Ratio	Amount of water (L/m^3 air)
25	0.032	80	0.0256	0.01612231	16.1223105
26	0.034	80	0.0272	0.01715775	17.1577506
27	0.036	80	0.0288	0.01819655	18.1965565
28	0.038	80	0.0304	0.01923874	19.2387445
29	0.04	80	0.032	0.02028433	20.2843312
30	0.042	80	0.0336	0.02133333	21.3333333
31	0.045	80	0.036	0.02291327	22.9132771
32	0.048	80	0.0384	0.024501	24.5010002
33	0.05	80	0.04	0.02556383	25.5638325
34	0.053	80	0.0424	0.02716465	27.1646495
35	0.056	80	0.0448	0.02877340	28.7734008
36	0.059	80	0.0472	0.03039014	30.3901454
37	0.063	80	0.0504	0.03255834	32.5583424
38	0.066	80	0.0528	0.03419397	34.1939716
39	0.07	80	0.056	0.03638756	36.3875686
40	0.074	80	0.0592	0.03859588	38.5958807
41	0.078	80	0.0624	0.04081905	40.8190566
42	0.082	80	0.0656	0.04305724	43.0572469
43	0.087	80	0.0696	0.04587633	45.8763313
44	0.091	80	0.0728	0.04814886	48.1488649
45	0.096	80	0.0768	0.05101137	51.0113727

Table 11. the amount of water present in 1 m^3 in different temperatures with 90 % *R.H*.

Temp. (°C)	Saturation Pressure (bar)	Relative Humidity (*RH* %)	Partial Pressure of water (bar)	Humidity Ratio	Amount of water (L/m^3 air)
25	0.032	90	0.0288	0.01819655	18.1965565
26	0.034	90	0.0306	0.01936925	19.3692566
27	0.036	90	0.0324	0.02054626	20.5462609
28	0.038	90	0.0342	0.02172759	21.7275931
29	0.04	90	0.036	0.02291327	22.9132771
30	0.042	90	0.0378	0.02410333	24.1033369
31	0.045	90	0.0405	0.02589668	25.8966847
32	0.048	90	0.0432	0.02770001	27.7000155
33	0.05	90	0.045	0.02890782	28.9078234
34	0.053	90	0.0477	0.03072797	30.7279789
35	0.056	90	0.0504	0.03255834	32.5583424
36	0.059	90	0.0531	0.034399	34.3990002
37	0.063	90	0.0567	0.03686937	36.8693743
38	0.066	90	0.0594	0.03873439	38.7343922
39	0.07	90	0.063	0.04123756	41.2375691
40	0.074	90	0.0666	0.04375978	43.7597845
41	0.078	90	0.0702	0.04630125	46.3012566
42	0.082	90	0.0738	0.04886220	48.8622066
43	0.087	90	0.0783	0.05209112	52.0911279
44	0.091	90	0.0819	0.05469673	54.6967306
45	0.096	90	0.0864	0.05798219	57.9821978

Table 12. the amount of water present in 1 m^3 in different temperatures with 100 % *R.H*.

Temp. (°C)	Saturation Pressure (bar)	Relative Humidity (*RH* %)	Partial Pressure of water (bar)	Humidity Ratio	Amount of water (L/m^3 air)
25	0.032	100	0.032	0.02028433	20.2843312
26	0.034	100	0.034	0.02159611	21.5961195
27	0.036	100	0.036	0.02291327	22.9132771
28	0.038	100	0.038	0.02423583	24.235837
29	0.04	100	0.04	0.02556383	25.5638325
30	0.042	100	0.042	0.02689729	26.8972973
31	0.045	100	0.045	0.02890782	28.9078234
32	0.048	100	0.048	0.03093084	30.9308469
33	0.05	100	0.05	0.03228653	32.28653
34	0.053	100	0.053	0.03433064	34.3306431
35	0.056	100	0.056	0.03638756	36.3875686
36	0.059	100	0.059	0.03845742	38.4574273
37	0.063	100	0.063	0.04123756	41.2375691
38	0.066	100	0.066	0.04333808	43.3380839
39	0.07	100	0.07	0.04615955	46.1595547
40	0.074	100	0.074	0.04900505	49.0050572
41	0.078	100	0.078	0.0518749	51.8748998
42	0.082	100	0.082	0.05476939	54.769396
43	0.087	100	0.087	0.05842267	58.4226721
44	0.091	100	0.091	0.06137381	61.373814
45	0.096	100	0.096	0.06509893	65.098937

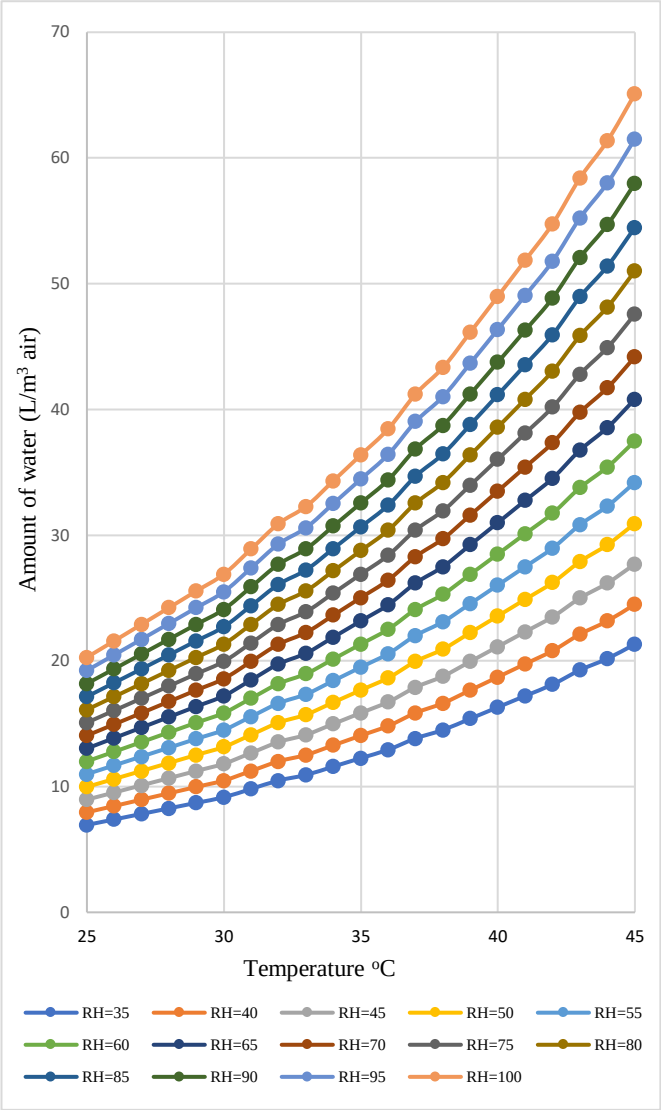

Fig. 14 amount of water present in 1m^3 of air at different temperature and different *R.H.*

4.3. Case 3 (Ansys case)

In this case, the simulation using Ansys/fluent for the experimental device and more cases are verified without cost and a long time to get more results. Twenty-four cases are studied using three inlet velocities of (0.25 m/s, 0.5 m/s, 0.75 m/s) with eight values for inlet temperature of (15, 20, 25, 30, 35, 40, and 50 °C) for relative humidity ranging from 35 to 100 % for each case. The results show that water production increases with a decrease in the air's velocity and increasing relative humidity and temperature. The contours of pressure, velocity, temperature, and humidity will be shown below.

4.3.1. Pressure

It is observed from the numerical results that the pressure drop of the airflow has approximately the same behavior for 24 studied cases as shown in Fig. 18, which showed the static pressure contours in the dehumidification duct as well as upstream and downstream flow. The static pressure contours at the duct downstream showed the existence of different pressure regions. The stationary pressure distribution on the cooled face is uniform.

4.3.2. Velocity

For three different inlet velocity which are (0.25, 0.5, and 0.75 m/s), and for different temperatures from (15 to 50 °C), the effect of velocity on the water production rate is studied. Water production rate increases when the air velocity decreases. The contours of velocity magnitude and path lines can be seen in Figs. 19, 20, and 21.

4.3.3. Temperature

Figures 22, 23, 24, and 25 represents the temperature variation contours in the cooler for different planes. The Iso-surface of temperature contours is decreased. The temperature distribution on the cold face of every case of the three cases is not uniform. In this region, the temperature is reduced to 283 K as decreased from a maximum of 300 K, which is related to inlet velocity, air temperature, and relative humidity.

4.3.4. Humidity

The relative humidity is observed from the 24 studied cases' numerical results. The mass fraction of the duct downstream is from 16 to 40 %. In the inlet, it has been 100 % on the cooled surface according to dew point activity. As a result, water production increases at max. humidity in the cooled shell, Fig. 26 shows the variation of water production rate with relative humidity. The water production rate increases with increasing relative humidity.

5. Conclusions

After analyzing all these aspects, it has been concluded that the thermoelectric refrigeration device can be used for the removal of moisture and water production. It has been further deduced that water production depends on the size of the thermoelectric device. Moreover, the best-operating regions are those that have high humidity and temperature. Also, solar energy can be sued as a power source for thermoelectric. Lastly, the most critical aspects of the enhanced environment mechanism through used filtration have been analyzed.

Nomenclature	
Symbol	**Description**
CFD	Computational Fluid Dynamics.
Exp.	Experimental.
Num.	Numerical.
ρ	Density.
v	Velocity vector.
Γ	Effective exchange coefficient of Ø.
$S_Ø$	Source rate per unit volume.
C	Case
V_s	Supply velocity
P	The pressure of the gas in Pa
V	The volume of the gas in m^3
m	The mass of the gas in kg
R	A constant of proportionality
T	The absolute temperature of the gas in K
P_v	The partial pressure of water vapor in saturated air
P_{sw}	Saturated pressure of vapor corresponding to wet bulb temperature from steam table
P_b	Barometric pressure
t_w	Wet bulb temperature
t_d	Dry bulb temperature

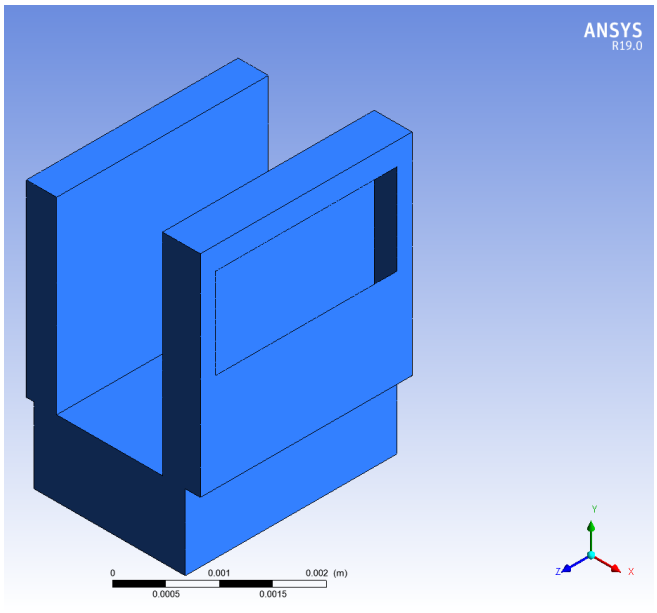

Fig. 15 domain in CFD post.

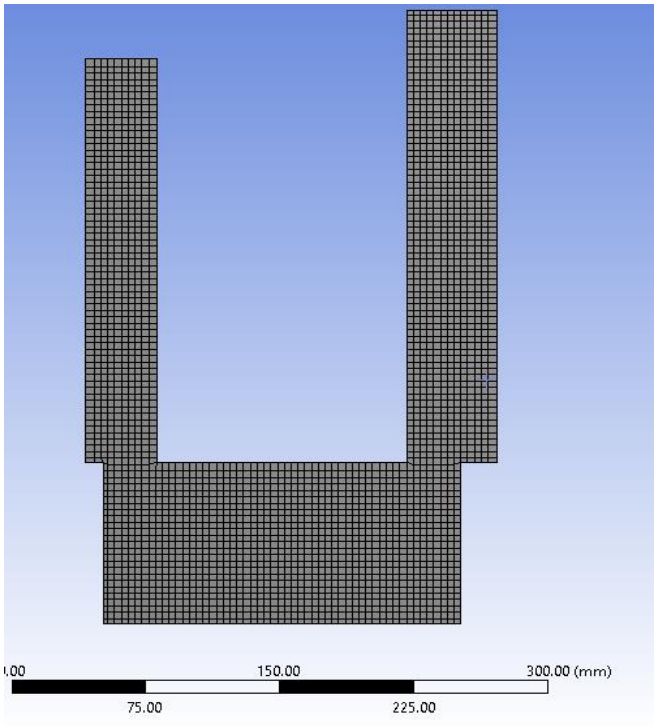

Fig. 16 side Mesh domain.

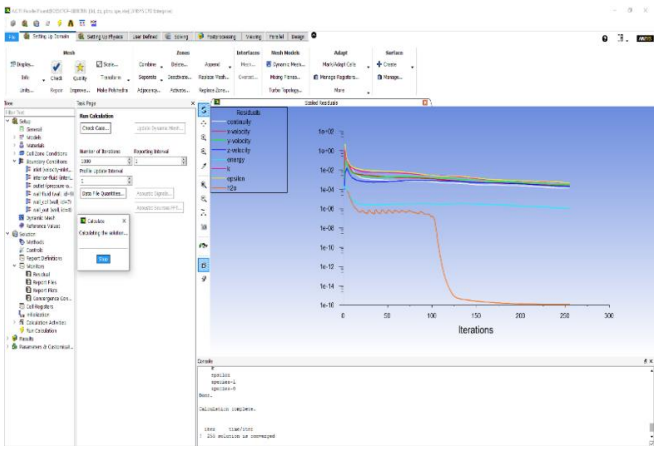

Fig. 17 iteration and convergence of the system.

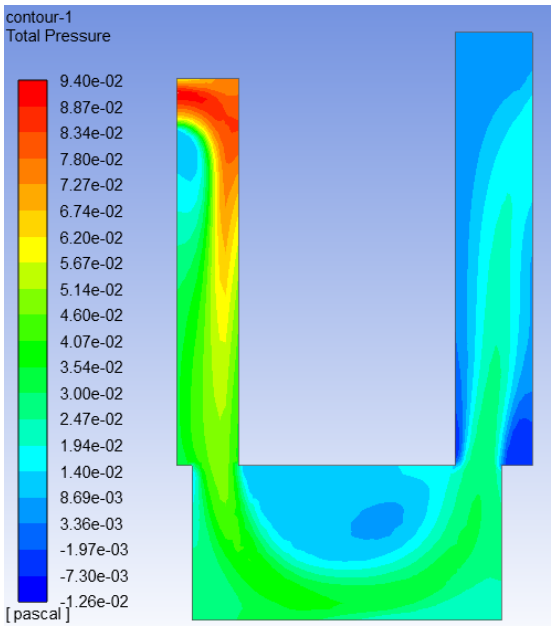

Fig. 18 contour of Static Pressure.

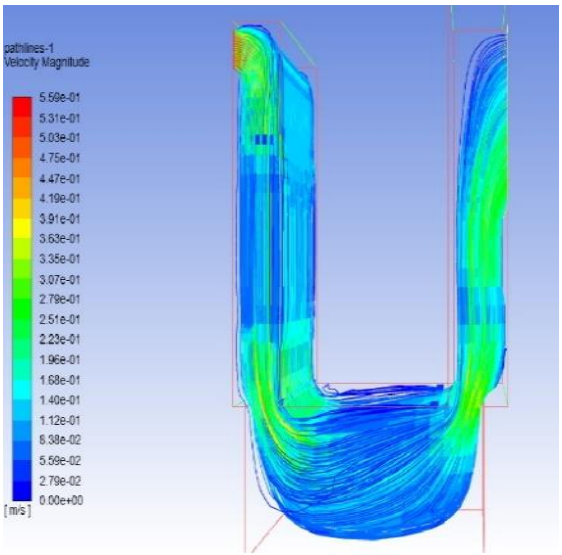

Fig. 19 path lines of velocity magnitude.

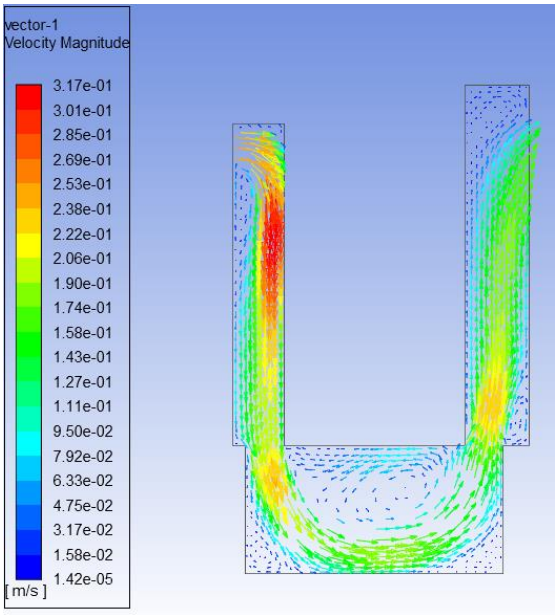

Fig. 20 vector 1 of velocity magnitude.

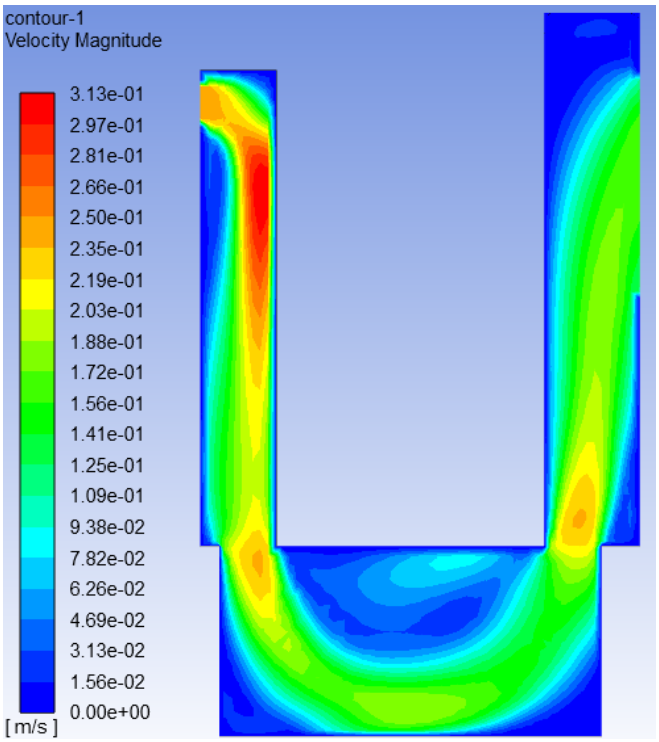

Fig. 21 contour of velocity magnitude.

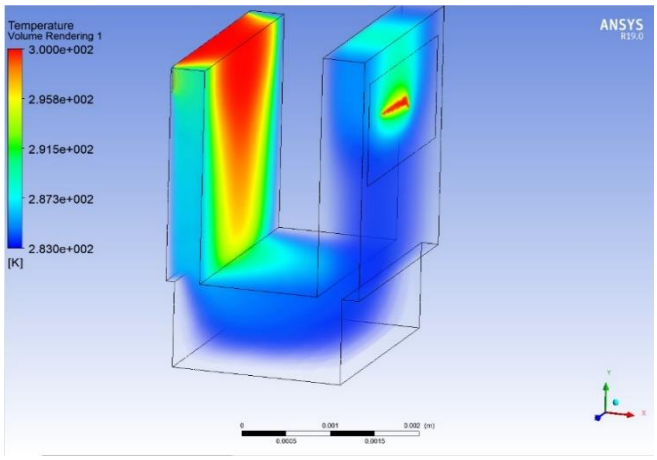

Fig. 22 volume rendering of temperature.

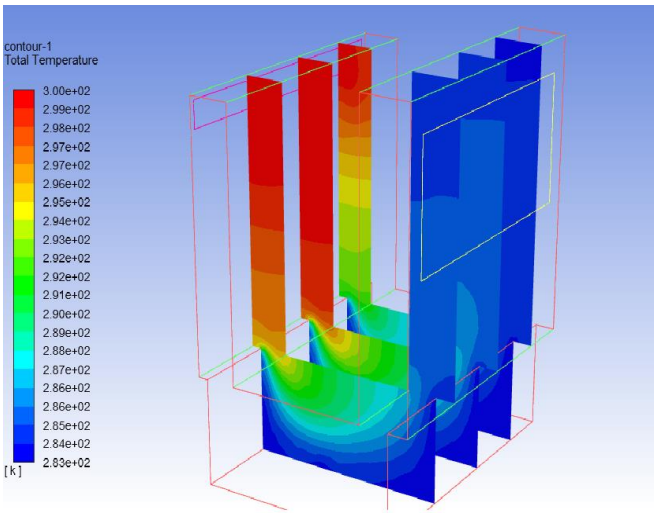

Fig. 23 contours of total temperature 1.

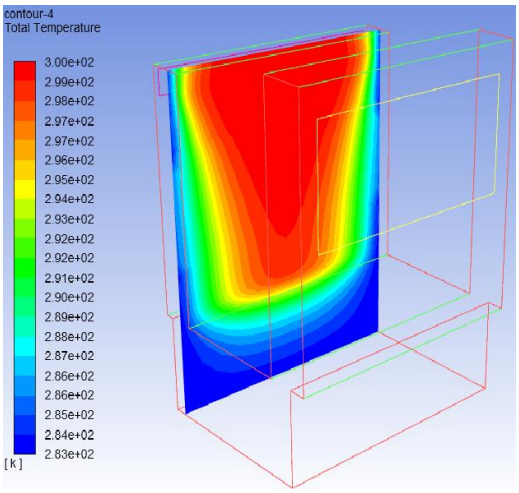

Fig. 24 contours of total temperature 2.

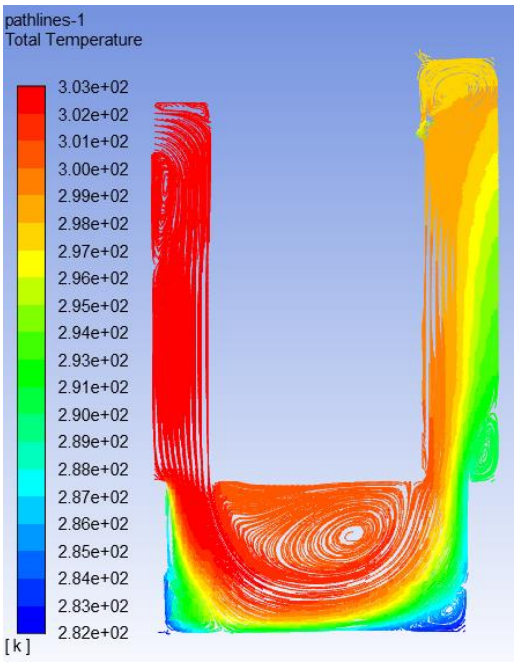

Fig. 25 path lines of total temperature.

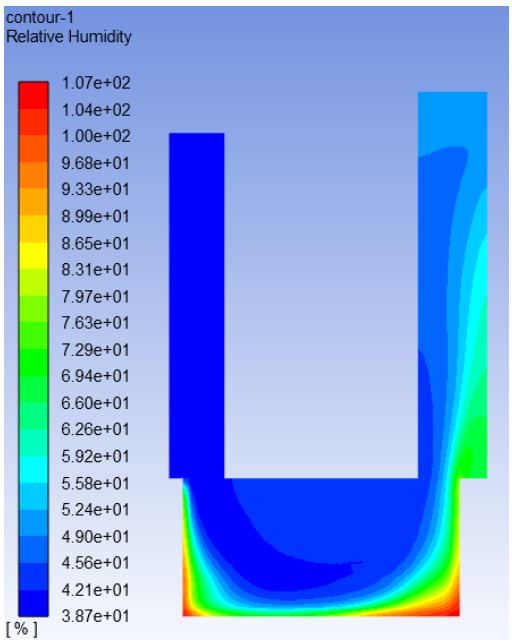

Fig. 26 contours of relative humidity.

References

[1] Turral Hugh, Jacob Burke and Jean-Marc Faurès, Climate Change, Water and Food Security, Food and Agriculture Organization of the United Nations (FAO), ISBN: 9789251067956, 2011.

[2] Scrivani Alessandro and Ugo Bardi, "A Study of the use of Solar Concentrating Plants for the Atmospheric Water Vapour Extraction from Ambient Air in the Middle East and Northern Africa Region", Desalination, Vol. 220, Issue 1-3, pp. 592-99, 2008. https://doi.org/10.1016/j.desal.2007.04.060.

[3] Janos J. Bogardi, David Dudgeon, Richard Lawford, Eva Flinkerbusch, Andrea Meyn, Claudia Pahl-Wostl, Konrad Vielhauer, and Charles Vörösmarty, "Water Security for a Planet under Pressure: Interconnected Challenges of a Changing World Call for Sustainable Solutions", Elsevier, Current Opinion in Environmental Sustainability, Vol. 4, Issue 1, pp.35-43, 2012. https://doi.org/10.1016/j.cosust.2011.12.002

[4] Dash Abhishek and Anshuman Mohapatra, "Atmospheric Water Generator: To Meet the Drinking Water Requirements of a Household in Coastal Regions of India", Bachelor of Technology Thesis, Department of Mechanical Engineering, National Institute of Technology, Rourkela Odisha-769008, India, 2015.

[5] A. E. Kabeel, Mohamed Abdulaziz, and Emad M.S. El-Said, "Solar Based Atmospheric Water Generator Utilization of a Fresh Water Recovery: A Numerical Study", Taylor and Francis, International Journal of Ambient Energy, Vol. 37, Issue 1, pp. 68-75, 2016. https://doi.org/10.1080/01430750.2014.882864

[6] Shanshan Liu, Wei He, Dengyun Hu, Song Lv, Delu Chen, Xin Wu, Fusuo Xu, and Sijia Li, "Experimental Analysis of a Portable Atmospheric Water Generator by Thermoelectric Cooling Method", Elsevier, Energy Procedia, Vol. 142, pp. 1609-1614, 2017. https://doi.org/10.1016/j.egypro.2017.12.538

[7] A. Bharath and K. Bhargav, "Design Optimization of Atmospheric Water Generator", International Journal for Research in Applied Science and Engineering Technology Vol. 5, No. 12, pp.572-578, 2017.

[8] Raihan Islam, Abu Saleh Musajjee, and S. M. Ullah, Iffatul Bushra Siddique, "Solar Powered Automated Atmospheric Water Generator Using Peltier Device", Degree of Bachelor of Science in Electrical and Electronic Engineering, BRAC University, Dhaka, 2017.

[9] H. K. Versteeg and W. Malalasekera, An Introduction to Computational Fluid Dynamics, Second Edition, Pearson Education Limited, Edinburgh Gate, Harlow, England, ISBN: 978-0- 13-127498-3, 2007.

[10] ANSYS Inc. users guide, version 19, 2019.

[11] Haywood and Richard Wilson, Thermodynamic Tables in Si (Metric) Units, Cambridge University Press, ISBN: 0521386934, 1990.

Biographies

Saleh E. Najim received Ph.D. in Mechanical Engineering (Energy and Combustion) from the University of Wales, the U.K. in 1979 and received the scientific title Professor from the Mechanical Engineering Department, College of Engineering, University of Basrah, Iraq in 1998. He worked as a Professor in Mechanical Engineering to teach and supervise undergraduate students, M.Sc., and Ph.D.

Hussein S. Sultan graduated B.Sc. in Mechanical Engineering in 1999, and received M.Sc. and Ph.D. Degrees (Thermal Mechanics) from the Mechanical Engineering Department, College of Engineering, University of Basrah, Iraq in 2001 and 2011 respectively. Recently Worked as Associate Professor in Mechanical Engineering to teach and supervise undergraduate students, M.Sc., and Ph.D.

Mohammed Alsheekh received a B.Sc. and M.Sc. degree in Mechanical Engineering (Thermal Mechanics) from the University of Basrah, College of Engineering, Basrah, Iraq, in 2000 and 2015 respectively. Currently works toward a Doctorate of Philosophy degree in Mechanical Engineering.